A new quasi-steady method to measure gas permeability of weakly permeable porous media

Yves Jannot, Didier Lasseux

REVIEW OF SCIENTIFIC INSTRUMENTS, 2012, **83**, 015113 (13pp), DOI: 10.1063/1.3677846

A new quasi-steady method to measure gas permeability of weakly permeable porous media

Yves Jannot[1] and Didier Lasseux[2,a)]

[1]*LEMTA, Nancy-Université, CNRS, 2, avenue de la Forêt de Haye, BP160, 54504 Vandoeuvre Cedex, France*
[2]*I2M, Université de Bordeaux, CNRS, Esplanade des Arts et Métiers, 33405 Talence Cedex, France*

(Received 8 September 2011; accepted 28 December 2011; published online 30 January 2012)

A new quasi-steady method for the determination of the apparent gas permeability of porous materials is presented in this paper along with the corresponding interpretative physical model derived from the unsteady flow equations. This method is mainly dedicated to the measurement of very low permeability of thin porous media, although thicker but more permeable samples may also be analyzed. The method relies on quasi-steady flow resulting from a (quasi) constant pressure maintained at the inlet face of the sample. Gas flow-rate, as low as 3×10^{-10} m^3/s, is determined from the record of pressure increase in a reservoir connected to the outlet face of the sample. An estimate of the characteristic time, t_c, to reach quasi-steady flow after imposing a constant pressure at the inlet is derived. It is validated by direct numerical simulations of the complete unsteady flow, clearly defining the required experimental duration for the method to apply. Experimental results obtained on rather permeable and thick rock samples are reported showing an excellent agreement of the measured permeability with that determined independently on the same sample whereas the experimental value of t_c is also in very good agreement with the predicted one. The method is further employed on a composite material sheet allowing the identification of an apparent gas permeability of about 10^{-23} m^2.

I. INTRODUCTION

Accurate gas-permeability determination of porous materials having permeabilities lower than 1 mD ($\sim 10^{-15}$ m^2) remains a tricky task. Above this typical value, a classical measurement technique on a homogeneous 1D sample consists in performing a stationary Darcy experiment.[1,2] This can be carried out using an experimental device as the one schematically represented in Figure 1.

From the measurement of the inlet volumetric flow-rate Q_0, pressure drop ΔP, and inlet pressure P_0 under steady flow conditions, gas permeability k can be deduced from the following relationship:[3]

$$\frac{\mu e Q_0 P_0}{S \Delta P} = k P_m. \tag{1}$$

To arrive at this result, the gas is supposed to be ideal while the flow is assumed to be isothermal and slow enough for inertial effects to be negligible. Moreover, compressibility effects are assumed to be significant at the sample scale only, not at the pore scale. An alternative method, that makes use of a variable charge, was proposed to measure concrete permeability,[4] neglecting, however, Klinkenberg effects (see below for this physical mechanism). Results obtained with the method were successfully compared with a technique developed earlier. This method however neglects air compressibility and makes use of a water column in a capillary as a pressure gauge. The meniscus, above which a low pressure is imposed to perform the measurement, might be subjected to evaporation that was not taken into account in the description.[5]

a)Author to whom correspondence should be addressed. Electronic mail: didier.lasseux@ensam.eu. Tel.: +33 556 845 403. Fax: +33 556 845 436.

While dealing with materials having low permeability, Klinkenberg effects may be significant.[6] They are the macroscopic signature of gas molecules collisions at pore walls which effects become non negligible compared to gas molecules/molecules collisions.[7] Their impact can be estimated with the Knudsen number $Kn = \lambda/l$, λ being the mean free-path of gas molecules at the pressure and temperature under consideration and l, a characteristic size at the pore scale. Typically, Klinkenberg effects are significant when Kn is in the range 0.01 to 1. In this range, they can be taken into account using a classical slip flow description at the pore-scale while at the macroscopic scale, they are characterized by a Klinkenberg coefficient b having the unit of pressure. When Kn is extremely small, i.e., when the Klinkenberg coefficient b of the gas and porous material under concern is much smaller than P_m, k in Eq. (1) can be identified as the intrinsic permeability k_l. However, when Klinkenberg effects are significant, k must be understood as the apparent gas permeability at P_m. The intrinsic permeability k_l and Klinkenberg coefficient b may then be determined from several experiments performed under stationary conditions but at different values of P_m using the analogue of Eq. (1),[8–11] namely,

$$\frac{\mu e Q_0 P_0}{S \Delta P} = k_l (P_m + b). \tag{2}$$

From a practical point of view, when the above described steady-state method is used on weakly permeable materials (typically for $k < 10^{-18}$ m^2 for example), difficulties appear to measure the gas flow rate with enough accuracy. In fact, since this flow rate can be extremely small, less than few cm^3 per hour, conventional gas flowmeters are inappropriate and more sophisticated methods, that are more difficult to implement,

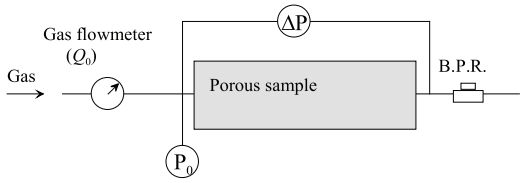

FIG. 1. Experimental set-up used to perform steady-state gas permeability measurement. B.P.R. is a back pressure regulator allowing to impose an outlet pressure.

must be envisaged. Time necessary to reach stationary flow, that can become extremely long due to its dependence on the inverse of the permeability as detailed below, has not been determined so far. An accurate estimate of this characteristic time is provided in this work.

The objective of the present work is to develop an alternative quasi-steady state method that is simple to implement, making use of an adequate flow-rate measurement technique. The corresponding interpretative model to determine gas permeability, derived from the complete unsteady flow model, is provided. An equivalent mass diffusivity is used yielding an accurate estimate of the characteristic time necessary to achieve quasi-steady flow in the proposed experimental procedure. This estimate is validated numerically from the solution of the complete unsteady flow model. As will be detailed below, the method is particularly well adapted, but not restricted, to thin and weakly permeable porous materials. Finally the method is illustrated with experimental results obtained on a thin composite material on the one hand and more permeable but much thicker rock samples on the other hand and on which both the intrinsic permeability and characteristic time of the quasi-steady regime are validated. The main advantages of the method are (i) the simplicity of the experimental device that can be carefully pre-designed by making use of the time limits and volume/pressure constraints that are detailed in this work; (ii) the simplicity of the interpretation of the measurement to derive the permeability (and eventually the Klinkenberg coefficient when the experiment is repeated at different pressure levels, just as with a pure steady-state experiment); (iii) the possible real-time control of the experiment by making use of the time limits and volume/pressure constraints required for the method to apply.

II. PHYSICAL MODEL AND THE NEW QUASI-STEADY METHOD

The basic idea of the technique developed in this work is inspired from non-stationary gas permeability measurement methods often referred to as "Pulse-Decay" or "Draw-Down" experiments and their variants.[12–21] In these methods, the inlet face of the sample is connected to a reservoir of volume V_0 while the outlet face is connected to a reservoir of volume V_1 which is finite for the Pulse-Decay or infinite (i.e., corresponds to the atmosphere) for the Draw-Down. A mass of gas is confined in the upstream reservoir at a larger pressure than the initial one in both the sample and downstream reservoir. At $t = 0$, the upstream reservoir is opened at the inlet edge of the sample letting the pressure pulse relax through the sample. From the record of the time evolution of the pressure in the upstream reservoir – or the pressure difference between the upstream and downstream reservoirs – the permeability and Klinkenberg coefficient can be identified by making use of the physical model detailed below.

A. Physical model

If we assume a homogeneous non-deformable sample and a 1D isothermal gas flow along the sample axis x at a very low Reynolds number – this is the case in practise – so that no significant inertial (or Forchheimer) effects are present,[10,22] the mass and momentum conservation equations are

$$\varepsilon \frac{\partial \rho(x,t)}{\partial t} + \frac{\partial(\rho(x,t)u(x,t))}{\partial x} = 0, \tag{3}$$

$$u(x,t) = -\frac{k}{\mu}\frac{\partial p(x,t)}{\partial x} = -\frac{k_l(1+b/p(x,t))}{\mu}\frac{\partial p(x,t)}{\partial x}. \tag{4}$$

In addition, if gas is considered as ideal ($p(x,t) = \rho(x,t)\frac{RT}{M}$), which is a valid approximation for gases like N_2 or He at experimental operating pressures of the order of ten bars, these two equations can be combined using the relationship between the apparent and intrinsic permeabilities $k = k_l(1 + b/p(x,t))$ yielding

$$\frac{\partial^2(p(x,t)+b)^2}{\partial x^2} = \frac{\varepsilon\,\mu}{k_l(p(x,t)+b)}\frac{\partial(p(x,t)+b)^2}{\partial t}, \tag{5}$$

or equivalently

$$\frac{\partial^2(p(x,t)+b)^2}{\partial x^2} = \frac{\varepsilon\,\mu}{k\,p(x,t)}\frac{\partial(p(x,t)+b)^2}{\partial t}. \tag{6}$$

When a completely unsteady experiment is considered, the upstream boundary condition (at $x = 0$) is such that the mass flow rate through the inlet face of the sample is exactly that out of the upstream tank. The mass flow rate through the inlet face is $-S\frac{p_0(t)M}{RT}\frac{k_l(1+b/p_0(t))}{\mu}\frac{\partial p(x,t)}{\partial x}|_{x=0}$, with $p_0(t) = p(x = 0, t)$, $p_0(t)$ being also the pressure in the upstream tank out of which the mass flow rate is $-\frac{V_0 M}{RT}\frac{dp_0(t)}{dt}$. Matching the two leads to

$$\frac{dp_0(t)}{dt} = \frac{S}{\mu V_0}k_l(p_0(t)+b)\frac{\partial p(x,t)}{\partial x} \quad \text{at } x = 0. \tag{7}$$

Following the same lines, the downstream boundary condition is given by

$$\frac{dp_1(t)}{dt} = -\frac{S}{\mu V_1}k_l\,(p_1(t)+b)\frac{\partial p(x,t)}{\partial x} \quad \text{at } x = e, \tag{8}$$

where $p_1(t)$ is the pressure at $x = e$ at t, i.e., in the downstream tank. The associated initial conditions are

$$p(x,0) = P_1 \quad \text{for } 0 < x \le e, \tag{9}$$

$$p(0,0) = P_0, \tag{10}$$

in which $P_1 = p_1(t = 0)$ and $P_0 = p_0(t = 0)$.

This model is a general one for 1D gas flow. Indeed, for a classical steady-state experiment, the stationary version of Eq. (5) can be integrated twice making use of the two bound-

ary conditions $p(x=0)=P_0$ and $p(x=e)=P_1$ yielding

$$p(x)=\left(\frac{(P_1+b)^2-(P_0+b)^2}{e}x+(P_0+b)^2\right)^{1/2}-b. \tag{11}$$

When this solution is introduced back in Darcy's law (Eq. (4)), the volume flow rate Q_0 at the entrance $x=0$ is readily obtained as

$$Q_0=u(0)\,S=-\frac{k_l}{\mu}\frac{(P_1+b)^2-(P_0+b)^2}{2\,e\,P_0}S, \tag{12}$$

which, when re-arranged, gives the result in Eq. (2).

In the case of a completely unsteady experiment, the model given by Eqs. (6)–(10) can be used in an inverse procedure in order to estimate k_l and b. This is achieved by minimizing the residual between the measured signal $p_0(t)$ (or $p_0(t)-p_1(t)$) and the corresponding one computed from the model as illustrated in Lasseux *et al.*[23] The method avoids major difficulties of the steady-state technique pointed out in the introduction, although the underlying physical model involves the porosity, ε, of the material. Because the simultaneous identification of the porosity with k_l and b in the inverse procedure is extremely difficult due to the poor sensitivity of the pressure decay signal to ε, this parameter must be known a priori and provided as an input for inversion. Moreover, it was shown in an earlier analysis that the input value of ε must be very accurate for a reliable estimate of k_l and b.[20] While dealing with weakly permeable materials having also frequently small porosity, the accurate determination of this parameter, which requires a separate dedicated experiment, is a difficult task. It must also be noted that the inverse process can be cumbersome so that the overall procedure makes a simpler method desirable. This is achieved with the method described below which takes advantage of both the steady and unsteady state techniques.

B. The new quasi-steady method

This method is inspired from the unsteady technique detailed above but, instead of letting the gas pressure pulse in the upstream reservoir relax through the sample, a constant pressure P_0 is maintained in V_0. This can be achieved either by continuously adjusting the pressure or more practically by simply choosing V_0 large enough so that, as can be easily inferred from Eq. (7), the variation δp_0 of $p_0(t)$ over the whole period of measurement remains extremely small compared to P_0. A criterion to satisfy this constraint is given in Sec. II C 2. Moreover, in this new method, we require the measurement of $p_1(t)$ to be performed at time $t>t_c$ (see Sec. II B 2 below for the estimation of t_c) so that the capacitive term in the right-hand side of Eq. (5) or (6) becomes negligible. This actually corresponds to the time necessary to reach steady flow when a constant pressure is applied at the inlet. Under these circumstances, the experiment is quasi-steady, the unsteady character remaining only through the time evolution of $p_1(t)$, as indicated by the boundary condition (8). The increase of $p_1(t)$ is actually recorded as an indirect measurement of the flow rate through the sample. A schematic representation of the experiment is reported in Figure 2. To keep the method simple, the focus is on the determination of the permeability that can be achieved in a straightforward manner from the downstream pressure record restricted to a period $t_c<t<t_f$, corresponding to a pressure increase δp_1 that remains small compared to P_1. The development of the method is proposed in the Sec. II B 1 and the associated constraint $t<t_f$ is made clear in Sec. II C 1.

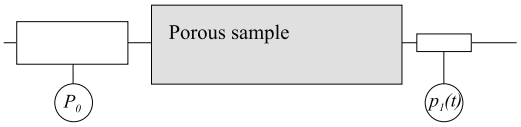

FIG. 2. Experimental configuration for the quasi-steady method.

1. Determination of the permeability

For $t>t_c$, (see Sec. II B 2 below for the estimation of t_c), the flow can be described by a quasi-steady version of the initial boundary value problem (6)–(10), in which the accumulation term in Eq. (6) is removed and the upstream boundary condition (7) is replaced by a constant pressure P_0 at $x=0$, hence yielding

$$\frac{\partial^2(p(x,t)+b)^2}{\partial x^2}=0, \tag{13}$$

$$p(0,t)=P_0, \tag{14}$$

$$\frac{dp_1(t)}{dt}=-\frac{1}{2}\frac{\mathrm{S}}{\mu V_1}k_l\frac{\partial(p(x,t)+b)^2}{\partial x}\quad \text{at } x=e. \tag{15}$$

The analytical solution of this problem can be simply written as

$$(p(x,t)+b)^2=-\frac{2\mu V_1}{\mathrm{S}\,k_l}\frac{dp_1(t)}{dt}x+(P_0+b)^2\quad 0\le x\le e, \tag{16}$$

which provides an expression for the rate of pressure increase in the downstream reservoir given by

$$\frac{dp_1(t)}{dt}=\frac{k_l\mathrm{S}}{2\mu V_1 e}((P_0+b)^2-(p_1(t)+b)^2). \tag{17}$$

This form could be used in an inverse procedure to identify k_l and b with the major drawback that the time derivative of the experimental record of $p_1(t)$ is required, making the technique inefficient. A much simpler and easy-to-use method can be derived, however, by noticing that, when $p_1(t)$ is recorded over a time interval $[t_c,\ t_f]$ such that the downstream pressure increment δp_1 is extremely small compared to P_1, $dp_1(t)/dt$ remains constant. Under these circumstances, the determination of the permeability can be made from a simple linear regression on $p_1(t)$ on the time interval $[t_0,\ t_1]$, $t_0\ge t_c$, $t_1\le t_f$, according to

$$k_l=2\frac{\mu V_1}{\mathrm{S}}\frac{e}{(P_0+b)^2-(P_1+b)^2}a$$
$$=\frac{\mu V_1}{\mathrm{S}}\frac{e}{(P_m+b)(P_0-P_1)}a. \tag{18}$$

TABLE I. Parameters employed in the numerical simulations.

Case nos.	k_l (m^2)	b ($\times 10^5$ Pa)	ε	e (mm)	P_0 ($\times 10^5$ Pa)	V_1 (m^3)	t_c (s) (Eq. (23))
1	10^{-16}	0	0.2	50	6	3×10^{-3}	150
2	10^{-18}	0	0.1	10	8	3×10^{-4}	225
3	10^{-19}	13.1	0.05	10	9	3×10^{-4}	276
4	10^{-20}	0	0.05	5	10	10^{-4}	2250
5	1.55×10^{-21}	30	0.05	5	10	10^{-4}	2250

Equivalently, since

$$k = k_l\,(1 + b/P_m)\,, \tag{19}$$

we have

$$k = 2\frac{\mu V_1}{\mathrm{S}}\frac{e}{P_0^2 - P_1^2}a = \frac{\mu V_1}{\mathrm{S}}\frac{e}{P_m\,(P_0 - P_1)}a, \tag{20}$$

where a is the slope of $p_1(t)$ estimated on the interval $[t_0,\ t_1]$. More precise forms can be used upon averaging Eq. (17) over the time interval on which a is estimated leading to $k_l = 2\frac{\mu V_1}{\mathrm{S}}\frac{e}{(P_0+b)^2-(\bar{p}_1+b)^2}a$ or $k = 2\frac{\mu V_1}{\mathrm{S}}\frac{e}{P_0^2-\bar{p}_1^2}a$ where $\bar{p}_1 = \frac{1}{t_1-t_0}\int_{t_0}^{t_1} p_1(t)\,dt$. For simplicity, the forms given by Eqs. (18) and (20) are kept in the sequel of the paper. Apart from the simplicity of the signal interpretation, it shall be noted that an evident advantage of the present method is that the mass flow rate, $\frac{V_1 M}{RT}\frac{dp_1(t)}{dt}$, which can be extremely small, is measured by recording $p_1(t)$ that can be performed accurately using rather standard pressure sensors.

As it is obvious from Eqs. (18) and (20), the method is such that a single experiment allows to estimate k only but not k_l and b separately. To estimate both parameters, several experiments, carried out at different pressures, are required as in the case of a steady experiment. For this reason, the method is particularly well suited to thin samples for which experiments are shorter due to the dependence of t_c on e^2 as shown in Sec. II B 2.

2. Characteristic time t_c and validation

In this section, we shall first determine the characteristic time for the quasi-steady flow hypothesis to hold and for the solutions (18) or (20) to apply. This is achieved from scaling arguments on the dimensionless form of the quasi diffusion equation (6). To do so, it is convenient to start from equation (6) of the complete unsteady model and let $\phi(x,\,t) = (p(x,\,t) + b)^2$ yielding

$$\frac{\partial\phi^*\,(x^*,\,t^*)}{\partial t^*} = D_m\frac{t_c}{e^2}\frac{\partial^2\phi^*\,(x^*,\,t^*)}{\partial x^{*2}}, \tag{21}$$

where D_m is a pseudo mass diffusivity that is pressure dependent. In Eq. (21), all quantities with the superscript * are dimensionless and obtained by scaling all variables by the corresponding characteristic reference value (noted below with the subscript c). In order to correctly identify the characteristic time t_c, associated to the propagation of the pressure signal through the sample, proper scalings on $\phi(x,\,t)$, $p(x,\,t)$ and x that make them $O(1)$ must be chosen. These scalings are given by $\phi_c = (P_0 + b)^2$, $p_c = P_0$ and $x_c = e$ yielding $D_m = \frac{k\,P_0\,p^*}{\varepsilon\,\mu}$. Since all the dimensionless variables in Eq. (21) are now $O(1)$, the pre-factor of the diffusive term must also be $O(1)$ yielding

$$D_m \sim \frac{k\,P_0}{\varepsilon\,\mu}, \tag{22}$$

and hence

$$t_c \cong \frac{\varepsilon\,\mu\,e^2}{k\,P_0} \cong \frac{\varepsilon\,\mu\,e^2}{k_l\,(1 + b/P_m)\,P_0}. \tag{23}$$

This last relationship represents an estimate of the criterion for the quasi-steady hypothesis to hold. Indeed, when the flow is observed at a time larger than t_c, the unsteady term in the left hand side of Eq. (21) becomes insignificant.

This prediction is now checked using direct numerical simulations performed on the complete unsteady model given by Eqs. (6)–(10). Details of the discrete procedure used to solve the problem are provided in Appendix A.

Numerical simulations were performed with values of the parameters reported in Table I using nitrogen ($\mu \cong 1.8 \times 10^{-5}$ Pa s) with $P_1 = 10^5$ Pa, a very large value of V_0 ($V_0 = 10^3$ m^3) ensuring a constant P_0 and $S = 1.96 \times 10^{-3}$ m^2. Values of the characteristic time t_c obtained from Eq. (23) are also indicated in this table. The Klinkenberg coefficient b was correlated to k_l according to an empirical relationship proposed in the literature, obtained for granular porous media in the range of permeability 10^{-15}–10^{-17} m^2 and given by[14]

$$b = 0.189\,k_l^{-0,36}. \tag{24}$$

Case 5 is such that all parameters are kept identical to Case 4 except k_l and b that were calculated to keep the term $k_l\,(1 + b/P_m)$ unchanged with respect to this later case. Under these conditions, the predicted value of t_c from Eq. (23) remains the same in both cases.

The evolution of $p_1(t)$ obtained from the numerical simulations is reported in Figure 3, for each of the four configurations under consideration while the corresponding evolutions of $dp_1(t)/dt$ are represented in Figure 4 in which the prediction of Eq. (17) in the quasi-steady regime was also reported as open symbols.

Results clearly show the three distinct regimes characterized by (i) the "pore-filling" period for which the downstream pressure remains unchanged at the very early stage of the experiment; (ii) a rapid evolution of $p_1(t)$ during a fully unsteady regime at intermediate times, up to $t = t_c$; (iii) the quasi-steady regime of particular interest in this work for times larger than t_c.

First, the evolution of $dp_1(t)/dt$ obtained from the numerical solution of the complete unsteady model is perfectly well predicted by the solution developed above (Eq. (17)) in the quasi-steady regime ($t > t_c$). Second, in this last regime

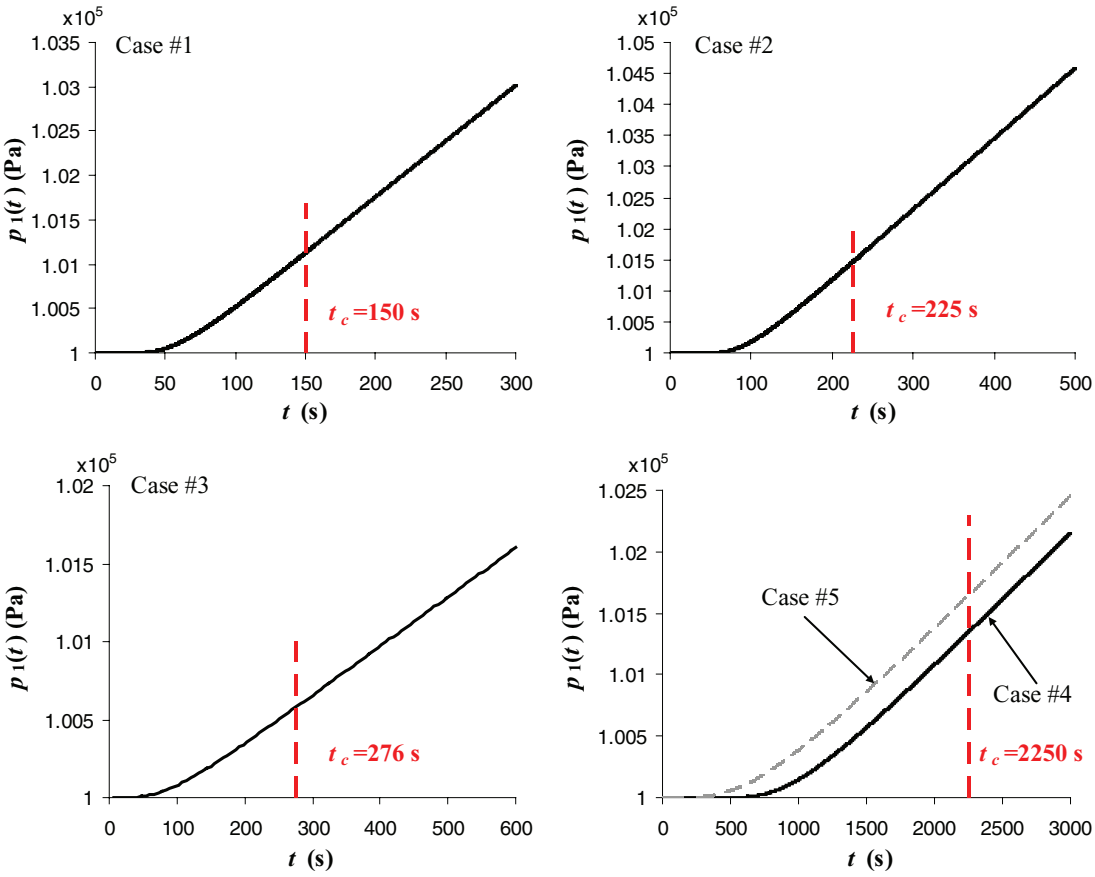

FIG. 3. (Color online) Evolutions of $p_1(t)$ in each of the five cases of Table I.

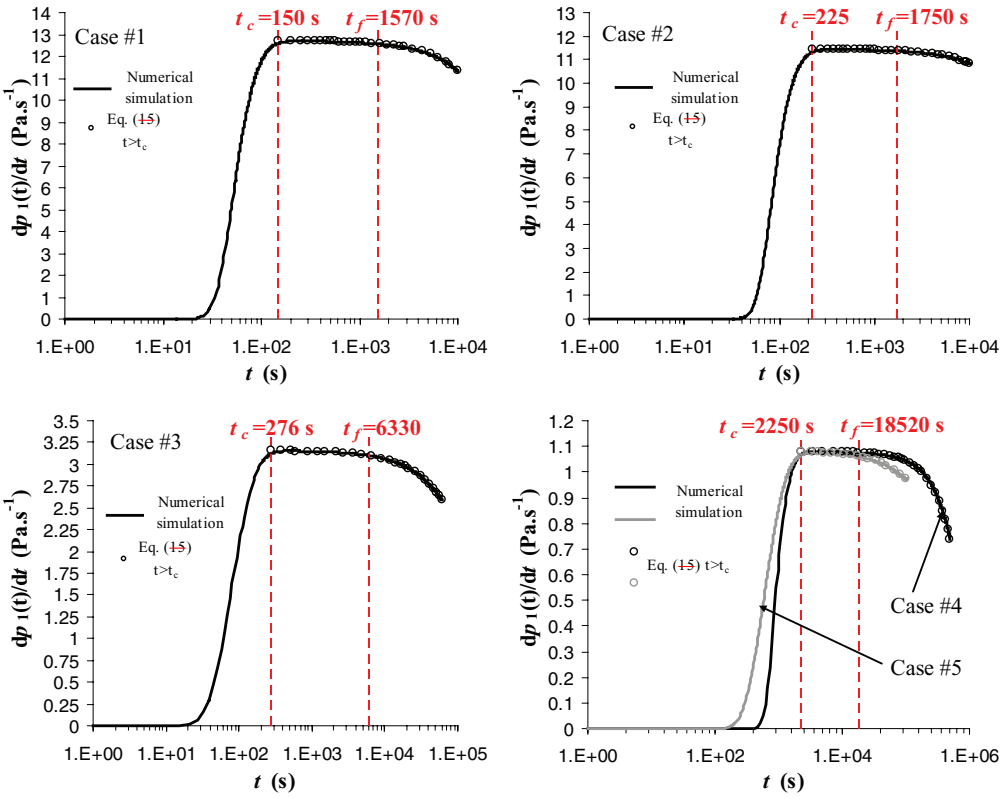

FIG. 4. (Color online) Evolutions of $dp_1(t)/dt$ in each of the five cases of Table I. The characteristic time t_c (see Sec. II B 2) and time constraint t_f (see Sec. II C 1) are materialised by the vertical dashed lines.

and $t \leq t_f$ (see Sec. II C 1 for this time constraint), p_1 evolves linearly, as shown in Figure 4, validating the use of Eqs. (18) and (20) to determine k_l and k. Finally, the characteristic time of the transient behaviour is perfectly well predicted by Eq. (23) as shown by the vertical dashed lines materialising the estimated values of t_c (see Figure 3). In particular, the excellent prediction of t_c, that remains unchanged for Cases 4 and 5, must be noted. As expected, t_c only depends on the characteristics of the sample and on the pressure levels P_0 and P_1. In particular it does not depend on V_1 (see Table I where several values of V_1 were considered). This validation confirms the physical relevance of the estimate for t_c which clearly highlights that the quasi-steady method developed in this work is better suited when $\varepsilon\, e^2/k_l$ is small in order to keep the experimental duration small.

C. Time t_f and upstream reservoir volume constraints

1. Time constraint t_f

The simple method of determination of k_l and k (Eqs. (18) and (20)) developed in this work requires that the downstream pressure increase δp_1 remains small compared to P_1 over the experimental observation of $p_1(t)$. This implies that the downstream pressure record must be restricted to the time interval $[t_c,\, t_f]$, corresponding to a quasi-linear evolution of $p_1(t)$. The time constraint t_f is now made explicit by noticing that $\frac{dp_1(t)}{dt} \cong \frac{k_l\,\mathrm{S}}{\mu V_1 e}\,(P_m+b)\,(P_0-P_1)$ for $t_c < t < t_f$ whereas $\frac{dp_1(t)}{dt}$ is increasing with time for $t < t_c$. As a consequence, δp_1 can be overestimated by writing

$$\delta p_1 < \frac{k_l \mathrm{S}}{\mu V_1 e}\,(P_m+b)\,(P_0-P_1)\,t_f. \tag{25}$$

The constraint $\delta p_1 \ll P_1$ can hence be safely expressed as

$$t_f \ll \frac{\mu V_1 e}{k_l\,\mathrm{S}}\,\frac{P_1}{(P_m+b)\,(P_0-P_1)} = \frac{\mu V_1 e}{k\,\mathrm{S}}\,\frac{P_1}{P_m\,(P_0-P_1)} = \frac{P_1}{a}. \tag{26}$$

As shown in Figure 4, the limit $t_f = 0.2\,\frac{\mu V_1 e}{k\,\mathrm{S}}\,\frac{P_1}{P_m(P_0-P_1)}$ materialized by dashed lines is a satisfactory criterion for all the situations under investigation.

It must be noted that the estimate of t_c and the constraint t_f can be used as a real-time feedback control of the experiment. Indeed, k can be determined from Eq. (20) on an interval $[t_0,\, t_1]$ where $p_1(t)$ is apparently linear while carrying out the experiment. An estimate of t_c (Eq. (23)) and the constraint (26) can be then post-compared to t_0 and t_1 to check the relevance of the permeability estimation and redefine the time interval $[t_0,\, t_1]$ if necessary while giving an indication on whether the experiment can be carried on. Note also that the expression of t_c along with the constraint (26) can be employed to pre-design the experimental setup when the permeability and porosity ranges to be investigated are defined.

2. Upstream volume constraint

When the experiment is performed with a fixed upstream volume V_0 to ensure a constant pressure P_0, this volume must be large enough for the simple quasi-steady method developed in this work to be effective which means that the pressure decrease δp_0 must remain small compared to P_0 for t up to t_f. The constraint can be made clear by estimating the corresponding mass of gas, δm, flowing out of the upstream reservoir over t_f. Over the time period t_f, a fraction δm_1 of this mass of gas contributes to the pressure rise in the downstream reservoir while the remaining part, δm_p, is accumulated in the pores to increment the pressure in the sample. An overestimate of δm_1 can be readily obtained from (25) and the assumption of an ideal gas leading to $\delta m_1 < \frac{k_l \mathrm{S}}{\mu\, e}\,(P_m+b)\,(P_0-P_1)\,t_f\,\frac{M}{RT}$. An overestimate of δm_p may be obtained by considering that gas accumulated in the pores corresponds to a pressure increase from P_1 to P_m yielding $\delta m_p < (P_m-P_1)\,\varepsilon\, e\, S\,\frac{M}{RT}$ so that an overestimate of the upstream pressure decrease $\delta p_0 = \frac{\delta m_1+\delta m_p}{V_0}\,\frac{RT}{M}$ can be expressed as

$$\delta p_0 < \frac{1}{V_0}\left(\frac{k_l \mathrm{S}}{\mu\, e}\,(P_m+b)\,(P_0-P_1)\,t_f + (P_m-P_1)\,\varepsilon\, e\, S\right). \tag{27}$$

In Appendix B, a more accurate estimate – but of less practical usefulness – of δm_p (and hence of δp_0) is derived.

The upstream constraint $\delta p_0/P_0 \ll 1$ ensuring quasi-steady conditions can finally be derived from Eq. (27) by requiring the following sufficient condition:

$$\frac{P_0-P_1}{P_0\,V_0}\left(\frac{k_l \mathrm{S}}{\mu\, e}\,(P_m+b)\,t_f + \frac{\varepsilon\, e\, S}{2}\right) = \frac{P_0-P_1}{P_0\,V_0}\left(\frac{k\,\mathrm{S}}{\mu\, e}\,P_m t_f + \frac{\varepsilon\, e\, S}{2}\right) \ll 1. \tag{28}$$

Again, this last constraint can be used either a posteriori to check the validity of a measurement or as a design guideline for an experimental setup to be used on given permeability-porosity intervals.

III. EXPERIMENTS

To illustrate the method described above, experimental results obtained on two different types of materials (rocks and composite material) are reported in this section. We focus on the determination of the apparent permeability, k, at a given pressure P_m, keeping in mind that k_l and b could be determined from repeated identical experiments at different values of P_m as documented elsewhere.[8–11]

A. Materials and method

The device used for the experiments is represented in Figure 5 and is composed of the following parts:

- A gas cylinder (N_2) is connected to the upstream reservoir through a pressure regulating valve V_D and a three-port valve V_3. This valve enables to connect the upstream reservoir either to the gas supply at P_0 or to the atmosphere.
- A digital manometer M1 (Keller LEO1) measures the pressure P_0 in the upstream reservoir.

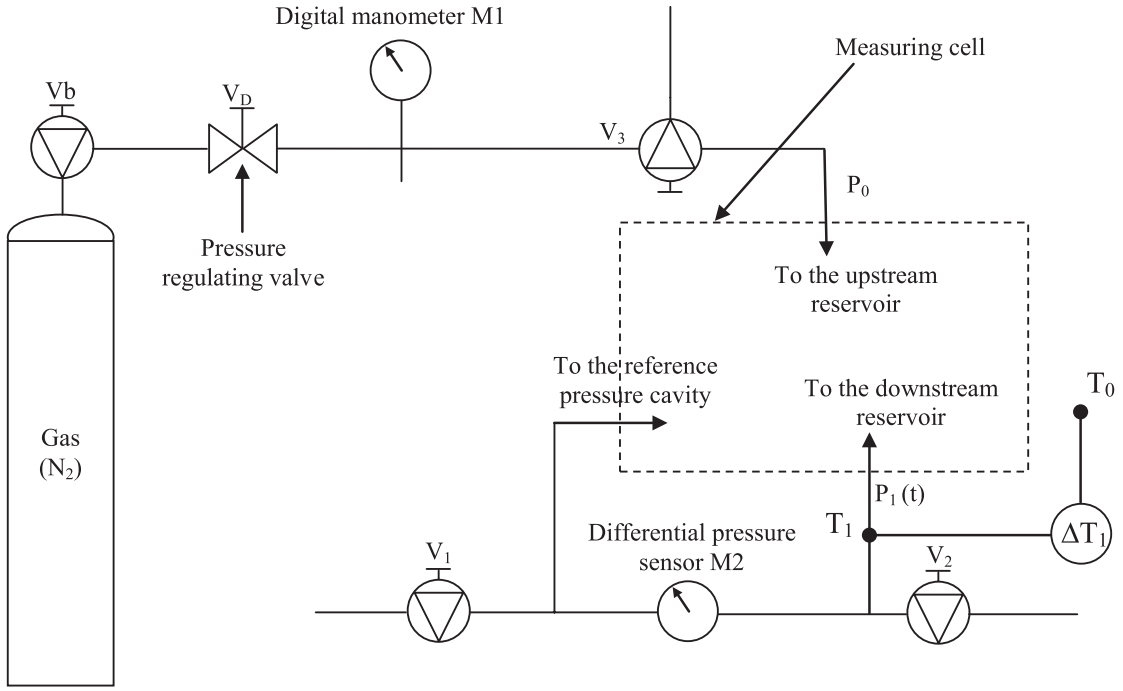

FIG. 5. Schematic representation of the experimental device. The measuring cell is one of those represented in Figure 6 depending on the sample type.

- A differential pressure sensor M2 (a Hottinger Baldwin Messtechnik 0–100 mbar for the experiment on the composite material and a Rosemount 3051S 0–620 mbar for experiments on rock samples) is employed to measure the pressure variation in the downstream reservoir. The high pressure input of the sensor is connected to the downstream reservoir and to a valve V_2 enabling the connection to the atmosphere. The low pressure input of the sensor is connected to a small chamber drilled in the sample holder, close to the downstream reservoir. The small chamber, that can be connected to the atmosphere through the valve V_1, is used as a reference pressure cavity that remains at the same temperature as the downstream chamber so that temperature perturbation are (partially) filtered out from the pressure signal recorded in the downstream reservoir. Moreover, potential atmospheric pressure fluctuations are also filtered out since the cavity remains closed during measurement.
- A digital data logger (Almemo 2290-5) records simultaneously the differential pressure, the temperature difference with respect to the enclosure, $\Delta T_1 = T_1 - T_0$, of the tubing connecting the volume V_1 to the high pressure input of the pressure sensor and the temperature difference with respect to the enclosure, $\Delta T_2 = T_2 - T_0$, of the sample holder, close to the reference pressure cavity. Temperatures are measured with type K thermocouples. Time sampling of the record can be varied in the range 0.1 s – 1h.

The measuring cell, materialized by the dashed area in Figure 5, was adapted to the type of sample under consideration. For the measurement on rock samples reported in Sec. III B 1, a Hassler sleeve core holder, represented in Figure 6(a), was used as usually employed for this type of sample.[24] In the case of the composite material sheet (see Sec. III B 2), the measuring cell schematized in Figure 6(b) was employed. In this last configuration, a plate of sintered porous material, which permeability (about 10^{-12} m^2) was much larger than that of the composite material, was placed below the composite sheet in the downstream reservoir. This plate avoids significant deformation of the composite material which would result from the applied pressure in the upstream reservoir and would bias the pressure rise record $p_1(t)$.

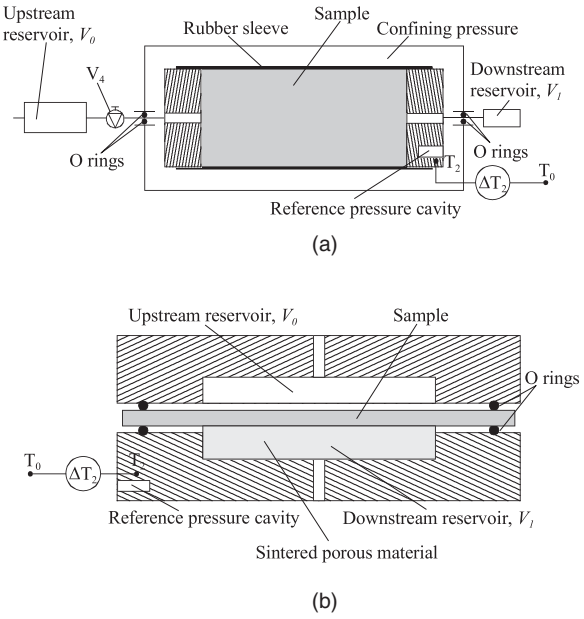

FIG. 6. Two measuring cells used for (a) a rock sample (Hassler sleeve core-holder); (b) a composite material sheet.

TABLE II. Characteristics of the rock samples R1 and R2.

Sample	k_l ($\times 10^{-17}$ m^2)	σ_{k_l} (%)	b ($\times 10^5$ Pa)	σ_b (%)	ε	e (mm)	S ($\times 10^{-3}$ m^2)
R1	3.8	0.05	1.16	0.42	0.055	60.3	1.134
R2	9.8	0.01	0.82	0.10	0.127	60.2	1.138

The operating process is the following:

- the sample is positioned into the device and a confining or clamping pressure is applied;
- the device is placed in a temperature controlled enclosure (typically at 30°C) while valves V_1, V_2 and V_3 (as well as V_4, (see Figure 6(a) for experiments on rock samples) are open to the atmosphere;
- valves V_1 and V_2 are closed when thermal equilibrium is reached and the atmospheric pressure is measured separately in the enclosure. Although equilibrium with the enclosure is reached, some low frequency temperature fluctuations (for instance on a day/night cycle for a long experiment) may still persist as will be further shown below on experiments carried out on the composite material;
- the pressure P_0 is set to the chosen value by adjusting the pressure regulating valve V_D;
- the valve V_3 is switched to connect the gas supply to the upstream reservoir. For experiments performed on rock samples, the valve V_4 (see Figure 6(a)) is closed. Recording of the downstream differential pressure and temperatures is started.

B. Experimental results

Experimental results were obtained on two different thick and relatively permeable rock samples. An additional result on a thin and very poorly permeable composite material sample is also reported to highlight the capability of the method to measure extremely small permeabilities.

1. Rock samples

The quasi-steady method was tested on two rock samples R1 and R2 which characteristics are reported in Table II. The samples were cylindrical cores of circular cross section and their characterization was made in the axial direction. For comparison purposes, the intrinsic permeability, k_l and Klinkenberg coefficient, b, were pre-determined independently from the present method using a fully unsteady (Draw-Down) method described above (see Sec. II A) and further detailed elsewhere.[20,21] Since the sensitivity of the upstream pressure decay signal, $p_0(t)$, to the porosity, ε, was poor, this parameter was measured with a classical gas pycnometry (N_2) experiment. The two parameters k_l and b were determined using an inverse procedure based on the physical model (6)-(10). Accuracy of the procedure is excellent since residuals on $p_0(t)$ (i.e., the difference between the measured signal and the simulated one at inversion convergence) are less than 100 Pa while the Draw-Down experiments were carried out with N_2 at P_0 up to 11×10^5 Pa and 16×10^5 Pa. Accuracy is corroborated by the relative standard deviation, σ_{k_l} and σ_b, on k_l and b reported in Table II.

Quasi-steady experiments were carried out with the parameters V_0, V_1, P_0, and P_1 reported in Table III where we have also indicated the times t_f at which experiments were ended. The expected apparent permeability, k, at these values of the pressures along with the corresponding expected characteristic time t_c reported in this table were estimated from data of Table II and Eqs. (19) and (23) respectively.

Experimental results of the evolution of $p_1(t)$ are represented in Figure 7 where the transient periods are clearly appearing followed by the quasi-steady periods.

In order to check the validity of the characteristic time estimates t_c reported in Table III, the time derivative $\frac{dp_1(t)}{dt}$ of the downstream pressure was determined. This was done from a polynomial least square fit of degree 6 (sample R1) and 4 (sample R2) performed on the signal $p_1(t)$. Evolutions of $\frac{dp_1(t)}{dt}$ are represented in Figure 8 in which we have also reported the predicted values of t_c as vertical dashed lines. These predictions are in excellent agreement with the emergence of the linear evolution of $p_1(t)$ characteristic of the quasi-steady regime observed experimentally, confirming the validity of the estimate. Moreover, the time derivative remains constant up to t_f for both experiments, confirming that permeability may be estimated following the quasi-steady model for $t > t_c$.

Next, apparent permeabilities were estimated from linear fits performed on $p_1(t)$ for $t_c \leq t \leq t_f$. The fits are represented in Figure 9 showing the relevance of the linear approximations over these time intervals with excellent determination coefficients. The slopes a were found to be 4.0 Pa s^{-1} (sample R1) and 9.4 Pa s^{-1} (sample R2), which upon using Eq. (20), yields $k \cong 5.15 \times 10^{-17}$ m^2 (sample R1) and $k \cong 12.12 \times 10^{-17}$ m^2 (sample R2). Again these two results are in excellent agreement with predicted values reported in Table III and validate the approach proposed in this work.

TABLE III. Experimental parameters for tests performed up to $t = t_f$ on rock samples R1 and R2. k and t_c are the expected apparent permeability at $(P_0 + P_1)/2$ and characteristic time of the transient period, both being evaluated from data of Table II.

Sample	V_0 ($\times 10^{-3}$ m^3)	V_1 ($\times 10^{-3}$ m^3)	P_0 ($\times 10^5$ Pa)	P_1 ($\times 10^5$ Pa)	k ($\times 10^{-17}$ m^2)	t_c (s)	t_f (s)
R1	1.02	2.26	5.96	1.02	5.08	120	1206
R2	1.02	2.26	6.04	1.02	12.14	116	2371

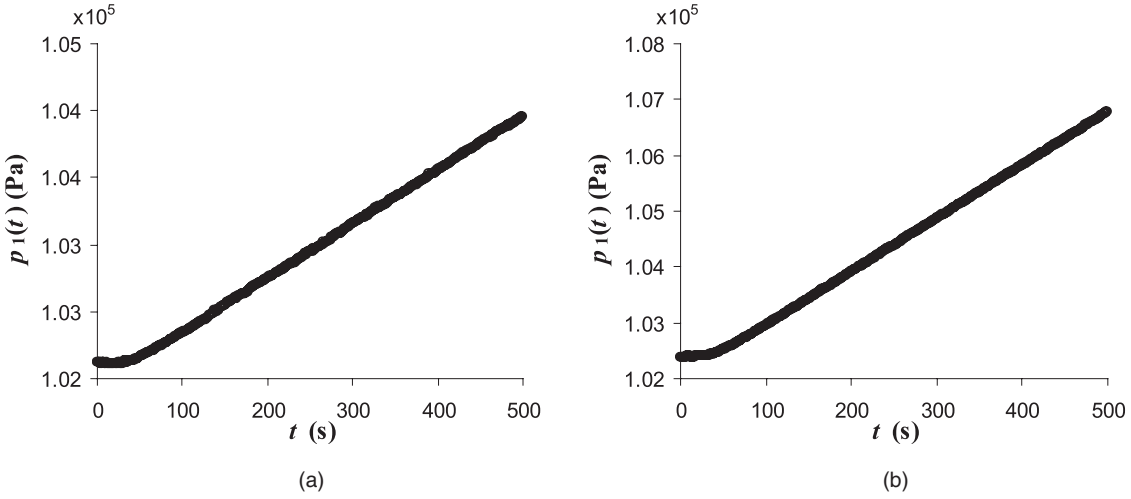

FIG. 7. Downstream pressure evolutions (a) sample R1; (b) sample R2. For convenience of the representation, the signal was truncated at $t = 500$s.

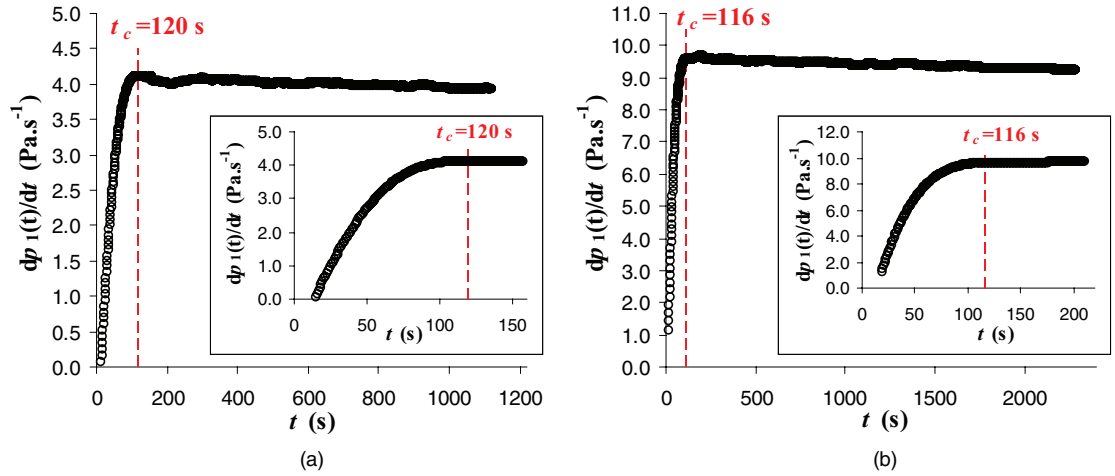

FIG. 8. (Color online) Evolution of the experimental downstream pressure time derivative. (a) sample R1; (b) sample R2. The characteristic times t_c predicted in Table III are materialised by the vertical dashed lines. *Insets*: same quantity restricted to early times (up to $t \cong 200$ s).

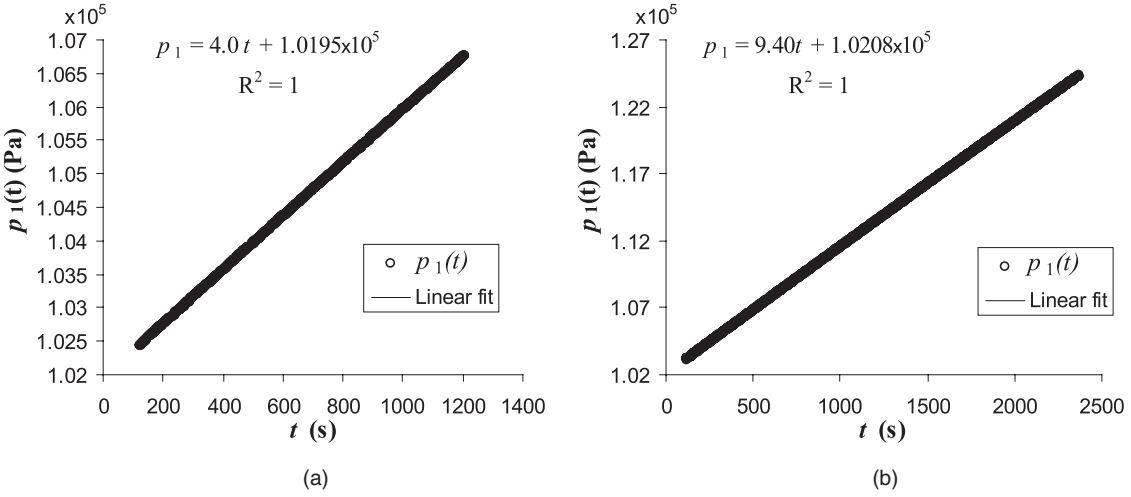

FIG. 9. Linear fits performed on the quasi-steady evolution of the downstream pressure $p_1(t)$, for $t_c \leq t \leq t_f$. (a) sample R1; (b) sample R2.

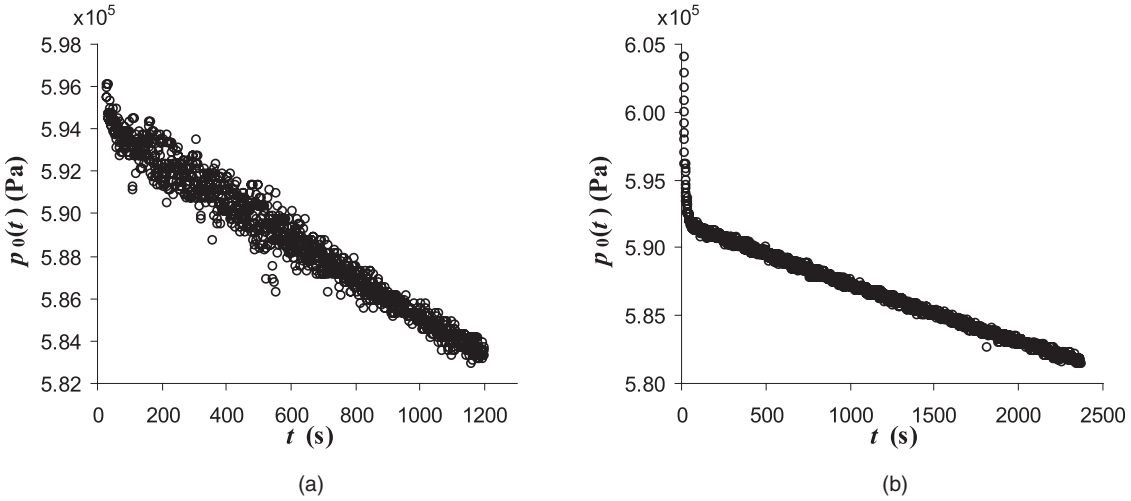

FIG. 10. Upstream pressure evolutions (a) sample R1; (b) sample R2.

Finally, the time and volume constraints expressed by the relationships (26) and (28) respectively may be checked a posteriori. According to our experimental parameters, the right hand side of the relationship (26) is roughly 2.53×10^4 s (sample R1) and 1.03×10^4 s (sample R2), values that are much larger than the values of t_f used to estimate k for both samples, confirming that the time constraint is fully satisfied. This is in agreement with observations made on Figure 8. Similarly, the left hand side in relationship (28) is evaluated to be approximately 1.96×10^{-2} (sample R1) and 9.01×10^{-2} (sample R2), both values being smaller than 1 which indicates that the experimental parameters were conveniently chosen for the quasi-steady experiment. In Figure 10, we have reported the evolutions of the upstream pressure for samples R1 and R2.

As can be inferred from these figures, the relative upstream pressure decrease, $\delta p_0/P_0$, is roughly 2.0×10^{-2} (sample R1) and 3.7×10^{-2} (sample R2). It is to be compared to the two values calculated from the left hand side of (28) and mentioned above which should be upper bounds. This is the case for sample R2, while, although experimental noise on $p_0(t)$ should be considered, it is not for sample R1. However, one must keep in mind that this upper bound is a restrictive one and when better estimated according to the expression provided in Appendix B, one finds 2.06×10^{-2} instead of 1.96×10^{-2} for sample R1 which better corresponds to the expected overestimate of $\delta p_0/P_0$.

2. Composite material sheet

An additional experiment was carried out to determine the transverse permeability of a thin and very poorly permeable medium, namely a sheet of composite glass-fiber/epoxy material. The experimental parameters were such that $e = 2$ mm, $S \cong 17.67 \times 10^{-3}$ m^2, $V_1 = 10^{-4}$ m^3, $P_0 \cong 6.08 \times 10^5$ Pa, $P_1 \cong 1.013 \times 10^5$ Pa. Since the upstream reservoir was directly connected to the gas cylinder through the valves V_d and V_3, V_0 can be considered as infinite in this experiment so that the constraint expressed by the relationship (28) is safely verified.

The time record of $p_1(t)$ obtained during this experiment is represented in Figure 11(a) while the evolution of the temperatures $\Delta T_1(t)$ and $\Delta T_2(t)$ are reported in Figure 11(b). As expected, the downstream pressure rise is very small (less

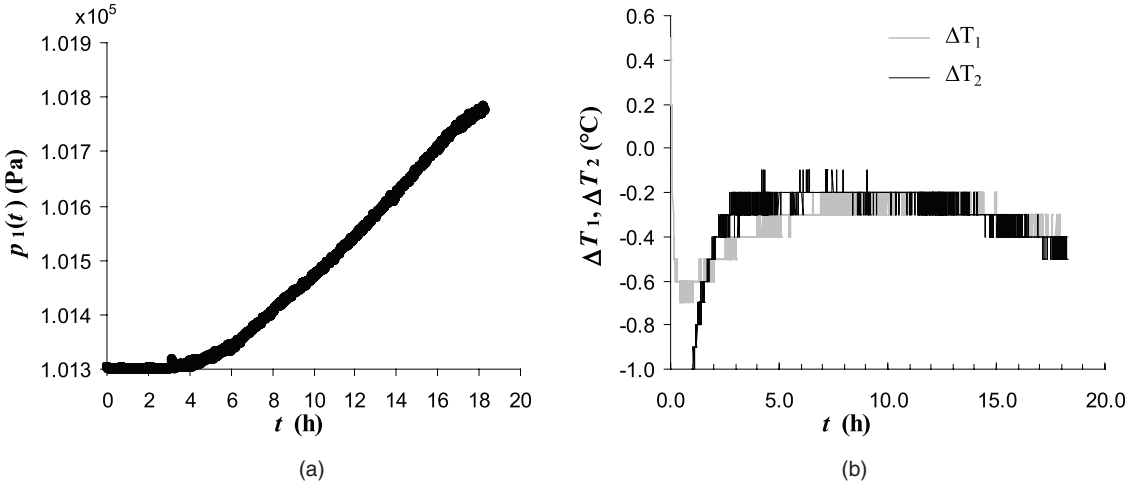

FIG. 11. Experimental results on the composite material sheet. Evolution of (a) the downstream pressure; (b) temperature differences ΔT_1 and ΔT_2.

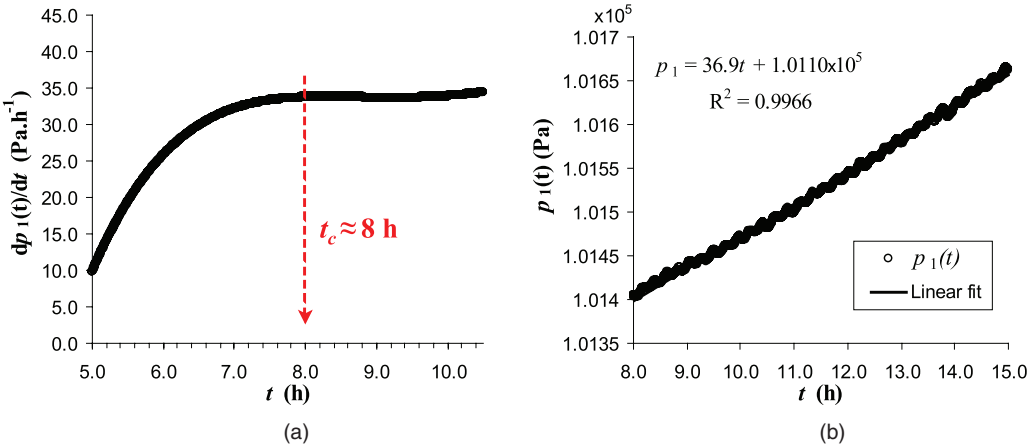

FIG. 12. (Color online) (a) Time derivative of the downstream pressure for $5 \leq t \leq 10$. (b) Least square linear fit on $p_1(t)$ for $8 \leq t \leq t_f = 15$: $a \cong 36.9$ Pa h^{-1}.

than 5 mbars over roughly 18 hours of record) suggesting that the permeability of the material is indeed extremely small. As can be seen in Figure 11(b), the temperatures remained relatively constant for $5.5 \leq t \leq 15$ h.

As for the data on the rock samples, a least square polynomial fit of degree 6 was performed on $p_1(t)$ in the interval of time $5 \leq t \leq 10$ h where the transition to the quasi-steady regime obviously occurs. The time derivative of this fit is depicted in Figure 12(a) indicating that t_c can be reasonably identified as $t_c \approx 8$ h. From this value, the slope a of $p_1(t)$ was identified in the time interval $8 \leq t \leq t_f = 15$ h (see Figure 12(b)) where the temperature is free of significant fluctuations yielding $a \cong 10^{-2}$ Pa s^{-1} with a very satisfactory determination coefficient. When reported in the expression (20) for the apparent permeability determined from this quasi-steady regime, one finds $k \cong 1.1 \times 10^{-23}$ m^2 which is far below the classical values of permeability determined with conventional measurement techniques. Note that the time constraint expressed by the relationship (26) is verified for this measurement. Indeed, the right hand side in (26) is evaluated to be $\sim 10^7$ s (i.e., $\sim$2900 h), which is much larger than the value of t_f used to estimate a, validating our experimental protocol for this material.

In the absence of data for the porosity of the material, no prediction of t_c can be performed. However, if ε is post-evaluated from the graphically identified value of t_c ($t_c \approx 8$ h), this yields $\varepsilon \approx 0.3\%$, a value that remains in the range of porosity reported in the literature for this type of material.[25,26]

IV. CONCLUSION

A method to determine the permeability of porous media, that is particularly well adapted to materials for which the ratio $\varepsilon e^2/k$ is small (ε is the porosity, e the sample thickness and k the apparent permeability of the material), i.e., to very poorly permeable porous media and/or thin samples, was proposed in this work. The method is based on the quasi-steady regime occurring during 1D flow when the sample is subjected to a (quasi) constant upstream pressure. The flow rate is indirectly measured through the pressure rise in the downstream reservoir, which is a net advantage of the technique. Indeed, since standard sensitive pressure sensors can be used, extremely small flow rates can be detected allowing the determination of very small permeabilities. The physical model to interpret the experiment was carefully derived from the complete unsteady model of flow showing that part of this quasi-steady regime is characterized by a linear evolution of the downstream pressure signal. A simple interpretation of this part of the signal can be made to determine the permeability and the Klinkenberg coefficient from repeated experiments at different mean pressure levels. Along with the fact that the experimental setup for this method is simple to implement, the simple interpretation makes the method of particular interest.

From scaling arguments, the characteristic time at which the quasi-steady regime is observed was explicitly derived. It was validated by numerical simulations of the complete unsteady model in a variety of operating conditions. This characteristic time defines the lower time-limit of the experimental downstream pressure signal to be considered with this method. The constraint on the upper time-limit was also determined, clearly defining the time interval of interest for the method to apply. Moreover, when the experiment is to be carried out with an upstream reservoir of finite volume, which is of practical common use, a constraint was provided for the method to remain valid. All these constraints can be advantageously used either as a set of guidelines to design an experiment and/or as a real time control tool to assert that the experiment is carried out under appropriate conditions.

Experiments carried out on two different rock samples were presented, demonstrating the validity of the method, both on the characteristic time of the quasi-steady regime and on the permeability estimates. The capability of the method to determine very low permeabilities (down to 10^{-23} m^2) was illustrated by a measurement in the transverse direction of a composite material sheet. This fast and simple method, taking advantage of both fully steady and unsteady techniques, is a promising tool for permeability characterization of very poorly permeable materials like samples of tight-gas or gas-shale reservoirs, cap rocks of gas or nuclear waste storage areas, sealing or composite materials, etc., all materials on which permeability measurement remained a challenging task so far and for which reliable and accurate methods are still scarce.

ACKNOWLEDGMENTS

The financial support from EDF is gratefully acknowledged.

We thank Sandra PROFICE for raising interesting questions that helped clarifying some developments in this paper.

APPENDIX A: NUMERICAL SCHEME FOR THE 1D UNSTEADY GAS FLOW

In this Appendix, we detail the numerical procedure used to solve the unsteady gas flow through the medium. The initial boundary value problem given by Eqs. (6)–(10) is first re-written using the pseudo-potential $\phi(x, t) = (p(x, t) + b)^2$ as

$$\frac{\partial^2\phi(x,t)}{\partial x^2} = \frac{\alpha}{\sqrt{\phi(x,t)}}\frac{\partial\phi(x,t)}{\partial t}, \tag{A1}$$

$$\frac{\partial\phi(x,t)}{\partial t} = \beta^{-1}\left(\sqrt{\phi(x,t)}\frac{\partial\phi(x,t)}{\partial x}\right) \quad \text{at } x = 0, \tag{A2}$$

$$\frac{\partial\phi(x,t)}{\partial t} = -\delta^{-1}\left(\sqrt{\phi(x,t)}\frac{\partial\phi(x,t)}{\partial x}\right) \quad \text{at } x = e, \tag{A3}$$

$$\phi(x,0) = (P_1 + b)^2 \quad \text{for } 0 < x \le e, \tag{A4}$$

$$\phi(0,0) = (P_0 + b)^2. \tag{A5}$$

These equations, where we have denoted $\alpha = \frac{\varepsilon\,\mu}{k_l}$, $\beta = \frac{\mu\,V_0}{k_l\,S}$, and $\delta = \frac{\mu\,V_1}{k_l\,S}$, are discretized using a finite difference scheme which is second order in space and a first order explicit Euler scheme in time. With the notation $\phi_i^n = \phi((i-1)\,\Delta x,\ (n-1)\,\Delta t)$, this scheme is given by

$$\phi_1^{n+1} = \frac{\Delta t}{2\,\alpha\Delta x + 3\beta}\sqrt{\phi_1^n}\frac{\phi_2^n - \phi_4^n + 4\phi_3^n - 4\phi_1^n}{2\Delta x} + \phi_1^n, \tag{A6}$$

$$\phi_i^{n+1} = \frac{\Delta t}{\alpha\,\Delta x^2}\sqrt{\phi_i^n}\left(\phi_{i+1}^n - 2\phi_i^n + \phi_{i-1}^n\right) + \phi_i^n \quad 2 < i < m-1, \tag{A7}$$

$$\phi_m^{n+1} = \frac{\Delta t}{2\alpha\Delta x + 3\delta}\sqrt{\phi_m^n}\frac{\phi_{m-1}^n - \phi_{m-3}^n - 4\phi_m^n + 4\phi_{m-2}^n}{2\Delta x} + \phi_m^n, \tag{A8}$$

where m is the number of space discretization nodes. Stability of the overall algorithm is subjected to a criterion on the time step due to the explicit character of the time scheme. This criterion is a classical one for a diffusion-like equation and is such that $\Delta t < min_i(\frac{\varepsilon\,\mu\,\Delta x^2}{2\,k_l(\phi_i)^{1/2}})$.

APPENDIX B: A MORE ACCURATE UPSTREAM VOLUME CONSTRAINT

An alternative and more accurate expression of the constraint given by the relationship (28) is developed in this Appendix.

We start from a mass balance of gas between $t = 0$ and $t = t_f$, given by

$$P_0V_0 + P_1(V_1 + \varepsilon\,e\,S) = (P_0 - \delta p_0)V_0 + (P_1 + \delta p_1)V_1 + \int_0^e \varepsilon\,S\,p(x,t_f)dx, \tag{B1}$$

While we shall overestimate δp_1 as

$$\delta p_1 < \frac{k_l S}{\mu V_1 e}(P_m + b)(P_0 - P_1)\,t_f = \frac{kS}{\mu V_1 e}P_m(P_0 - P_1)\,t_f, \tag{B2}$$

the expression $p(x, t)$ can be extracted form Eqs. (16) and (17) to give

$$p(x,t_f) = \left[(P_0+b)^2 - 2\frac{p_1(t_f)+b}{P_1+b}\frac{(P_m+b)(P_0-P_1)}{e}x\right]^{1/2}. \tag{B3}$$

Noticing that $p_1(t_f) = P_1 + \delta p_1$ while $\frac{\delta p_1}{P_1+b} \ll 1$, the integral term in Eq. (B1) can be explicitly calculated as $\int_0^e \varepsilon\,S\,p(x,t_f)dx \cong \frac{2}{3}\varepsilon\,e\,S\frac{(P_0+b)^3-(P_1+b)^3}{(P_0+b)^2-(P_1+b)^2}$. When inserted back into (B1) while taking into account the upper bound of δp_1 in (B2), one obtains an overestimate of δp_0 as

$$\delta p_0 < \frac{1}{V_0}\left(\frac{kS}{\mu\,e}P_m(P_0 - P_1)\,t_f + \varepsilon\,e\,S\left(\frac{2}{3}\frac{(P_0+b)^3 - (P_1+b)^3}{(P_0+b)^2 - (P_1+b)^2} - P_1\right)\right), \tag{B4}$$

and hence an alternative form to (28) developed in the paper given by

$$\frac{1}{P_0V_0}\left(\frac{kS}{\mu\,e}P_m(P_0 - P_1)\,t_f + \varepsilon\,e\,S\left(\frac{2}{3}\frac{(P_0+b)^3 - (P_1+b)^3}{(P_0+b)^2 - (P_1+b)^2} - P_1\right)\right) \ll 1. \tag{B5}$$

Although this form is more accurate than (28) and can be easily shown to be less restrictive, it is not of real practical usefulness. Indeed, since it involves the value of b which is not known while performing the measurement of k at a given P_m, a real-time feedback control of the validity of the experiment is impossible with this form.

Nomenclature

a	slope of $p_1(t)$ in the linear quasi-steady regime (Pa/s)
b	Klinkenberg coefficient (Pa)
D_m	pseudo mass diffusivity ($D_m = k\,P_0\,p^*/\varepsilon\,\mu$) (m^2/s)
e	sample thickness (m)
k	apparent gas permeability (m^2)
k_l	intrinsic permeability (m^2)
l	characteristic length at the pore scale (m)
M	molar mass of gas (kg/mol)
$p(x, t)$	pressure at x and t (Pa)

$p_0(t)$	absolute pressure in the upstream reservoir at t (Pa)
$p_1(t)$	absolute pressure in the downstream reservoir at t (Pa)
P_0	initial absolute pressure in the upstream reservoir ($=p_0(t=0)$) (Pa)
P_1	initial absolute pressure in the downstream reservoir ($=p_1(t=0)$) (Pa)
P_m	arithmetic mean pressure ($P_m=(P_0+P_1)/2$) (Pa)
Q_0	volumetric flow-rate ($m^3\ s^{-1}$)
R	ideal gas constant ($R=8.314$ J/mol/K)
S	sample cross sectional area (m^2)
t	time (s)
t_c	characteristic time to reach the quasi-steady regime (s)
t_f	final time of the experiment (s)
T	temperature (K)
$u(x,t)$	filtration velocity (m/s)
V_0	volume of the upstream reservoir (m^3)
V_1	volume of the downstream reservoir (m^3)
x	coordinate along the sample axis (m)

Greek

δp_0	pressure variation in the upstream reservoir over t_f (Pa)
δp_1	pressure variation in the downstream reservoir over t_f (Pa)
ΔP	pressure drop ($=P_0$-P_1) (Pa)
ΔT_1	temperature difference between the temperature-controlled enclosure and the tubing connecting V_1 to the pressure sensor ($\Delta T_1=T_1-T_0$) (K)
ΔT_2	temperature difference between the temperature-controlled enclosure and the sample holder, close to the reference pressure cavity ($\Delta T_2=T_2-T_0$) (K)
ε	porosity
ϕ	pseudo potential ($\phi=(p+b)^2$) (Pa^2)
λ	mean free-path of gas molecules (m)
μ	gas dynamic viscosity (Pa s)
ρ	gas density (kg/m^3)

Subscripts

0	upstream condition
1	downstream condition

Superscripts

*	dimensionless form

[1] V. Picandet, A. Khelidj, and G. Bastian, Cem. Concr. Res. **31**(11), 1525 (2001).
[2] S. Takeuchi, S. Nakashima, and A. Tomiya, J. Volcanol. Geotherm. Res. **177**(2), 329 (2008).
[3] R. D. Wyckoff, H. G. Botset, M. Muskat, and D. W. Reed, Rev. Sci. Instrum. **4**, 394 (1933).
[4] M. P. Yssorche, J. P. Bigas, and J. P. Ollivier, Mater. Struct. **28**, 401 (1995).
[5] J. J. Kollek, Mater. Struct. **22**, 225 (1989).
[6] L. J. Klinkenberg, API Drilling and Production Practice 200 (1941).
[7] P. C. Carman, *Flow of Gases through Porous Media* (Butterworths, London, 1956).
[8] Y. S. Wu, K. Pruess, and P. Persoff, Transp. Porous Media **32**, 117 (1998).
[9] J. A. Rushing, K. E. Newsham, P. M. Lasswell, J. C. Cox, and T. A. Blasingame, "Klinkenberg-corrected permeability measurements in tight gas sands: Steady-state versus unsteady-state techniques," presented at the *SPE Technical Conference and Exhibition*, Houston, Texas, 26–29 September 2004.
[10] V. Blanchard, D. Lasseux, H. Bertin, T. Pichery, G. Chauveteau, R. Tabary, and A. Zaitoun, SPE Res. Eval. & Eng. **10**(4), 423 (2007).
[11] S. Li, M. Dong, and Z. Li, J. Pet. Sci. Eng. **65** 81 (2009).
[12] G. H. Bruce, D. W. Peaceman, and H. H. Rachford, Petroleum Transactions, AIME **198**, 79 (1953).
[13] J. S. Aronofsky, C. G. Wallick, and P. P. Reichertz, *Method of Measuring Characteristics of Porous Materials*, Patent US 2867116 A, (1959).
[14] S. C. Jones, SPE Journal **12**(5), 383 (1972), http://www.onepetro.org/mslib/app/Preview.do?paperNumber=00003535&societyCode=SPE.
[15] P. A. Hsieh, J. V. Tracy, C. E. Neuzil, J. D. Bredehoeft, and S. E. Silliman, Int. J. Rock Mech. Min. Sci. Geomech. Abstr. **18**, 245 (1981).
[16] C. E. Neuzil, C. Cooley, S. E. Silliman, J. D. Bredehoeft, and P. A. Hsieh, Int. J. Rock Mech. Min. Sci. Geomech. Abstr. **18**, 253 (1981).
[17] D. Trimmer, Rev. Sci. Instrum. **53**(8), 1246 (1982).
[18] S. C. Jones, SPE Formation Evaluation **12**(1), 19 (1997), http://www.onepetro.org/mslib/app/Preview.do?paperNumber=00028450&societyCode=SPE.
[19] Y. Jannot, D. Lasseux, G. Vizé, and G. Hamon, in Symposium of the Society of Core Analysts, Calgary, 10–13 September 2007, SCA2007-08.
[20] Y. Jannot, D. Lasseux, L. Delottier, and G. Hamon, in Symposium of the Society of Core Analysts, Abu Dhabi, 29 October–2 November 2008, SCA2008-09.
[21] D. Lasseux, P. Jolly, Y. Jannot, E. Sauger, and B. Omnes, J. Pressure Vessel Technol. **133**(4), 041401 (2011).
[22] D. Lasseux, A. A. Abbasian Arani, and A. Ahmadi, Phys. Fluids **23**(7), 073103 (2011).
[23] D. Lasseux, P. Jolly, Y. Jannot, E. Sauger, and B. Omnes, paper presented at the Pressure Vessels and Piping Conference, Prague, 26–30 July 2009, PVP2009-77659.
[24] S. Al-Hinai, Q. J. Fisher, B. Al-Busafi, P. Guise, and C. A. Grattoni, Mar. Pet. Geol. **25**(6), 473 (2008).
[25] V. Fano, I. Ortalli, and K. Pozela, Biomaterials **16**, 1291 (1995).
[26] L. Lin, M. Luo, H. T. Tian, X. M. Li, and G. P. Guo, paper presented at the 17th World Conference on Non-Destructive Testing, Shanghai, China, 25–28 October 2008.